Effect of Graphene Oxide Treatment on the Properties of Cellulose Nanofibril Films Made of Banana Petiole Fibers

Changyan Xu,[a] Guangjing Wang,[a] Cheng Xing,[b] Laurent M. Matuana,[b] and Handong Zhou [a,*]

In this study, banana petiole-based cellulose nanofibril (CNF) films treated with graphene oxide (GO) were prepared and evaluated by means of Fourier-transform infrared (FTIR) spectroscopy, scanning electron microscopy (SEM), dynamic mechanical analysis (DMA), and thermogravimetric analysis (TGA). Tensile strengths (TS), dynamic mechanical properties, and thermal stabilities of the films were affected positively when the GO loading was less than 4.4 wt%. From these results, FTIR spectra, and SEM analyses, a strong coupling between the GO and the cellulose matrix could be concluded at lower GO loadings. The TGA and DMA results also suggested that the CNF film treated with 4.4 wt% GO had more char residue, better thermal stability, higher storage modulus, and higher retention ratio when compared to that without treatment. This work provides a new approach for more effective utilization of banana petiole as a feedstock for CNF and GO/CNF composites.

INTRODUCTION

The banana plant grows widely all over the world. Its residues, which are continuously increasing, result in serious pollution, due to either being dispersed in the planting area or being burned. Now, banana residues are being considered an ideal raw material for their natural fiber because they are renewable, biodegradable, and biocompatible. Zuluaga *et al.* (2009) isolated cellulose microfibrils (CMFs) with a diameter of 3 to 5 nm from the vascular bundles of banana rachis that were treated with alkali alone or alkali and peroxide, while Elanthikkal *et al.* (2010) obtained a stable aqueous suspension of CMFs from banana residues by treating them with alkali. Alternatively, Deepa *et al.* (2011) used a steam explosion treatment to extract cellulose nanofibers (CNFs) from banana residues. The obtained CMFs or CNFs have already been used as a component in composites (Jandas *et al.* 2013). Recently, graphene oxide (GO), as a possible intermediate for manufacture of graphene in large volume, has attracted much attention. Containing π-conjugated sp^2 domains and oxygenated sp^3 domains, GO shows semi-conductive properties, has large surface area, and has strong mechanical strength (Li *et al.* 2012; Tang *et al.* 2012). The large amount of oxygen-containing functional groups in GO, such as epoxy, hydroxyl, and carboxyl groups, as well as its

layer structure, make it hydrophilic and easily dispersible in water and other solvents (Kovtyukhova *et al.* 1999; Paredes *et al.* 2008; Wang *et al.* 2011; Shao *et al.* 2012). The ordered alignment in the polymer matrix by the π–π conjugation effect and the hydrogen bonds between the GO nanosheets and the polymer chains result in ordered nanofiller-matrix interactions at the molecular level; these interactions between the components have resulted in remarkable improvements to the composite's property at low filler concentrations (Park *et al.* 2008; Han *et al.* 2011; Wang *et al.* 2012).

In order to combine with the advantage of nanocellulose and graphene, many studies have been carried out. Graphene's intrinsic low weight and excellent thermal stability provide a good combination with chitosan, which can make composite materials with excellent antibacterial property (Lim *et al.* 2012). Gao *et al.* (2013) used cellulose nanofibers as the substrate to make cellulose nanofibers/reduced graphene oxide paper, which had flexible, transparent, and conductive properties, by layer-by-layer self-assembly method. Wang *et al.* (2014) prepared free-standing graphene oxide-carboxymethyl cellulose composite films with an ultrasonic mixing method; the resulting materials had nonlinear optical performance, such that they can be considered as a potential candidate for optical limiting applications. In the preparation of GO/cellulose composite films, the common solvents are NMMO (N-methylmorpholine-N-oxide) (Kim *et al.* 2011), ionic liquid 1-butyl-3-methylimidazolium chloride (Wang *et al.* 2012), and NaOH/urea aqueous (Han *et al.* 2011a) solution. At the same time, mechanical mixing also can be used (Yadav *et al.* 2013).

There are no reports found in the literature about the combination of CMFs or CNFs obtained from banana petiole and GO to form a new composite. In this study, we investigated the effects of GO on the properties of GO-treated CNF films made from banana petiole.

EXPERIMENTAL

Materials

Natural graphite powder (40 μm) was obtained from Qingdao Henglide Graphite Co., Ltd. (China). Laboratory grade concentrated H_2SO_4 (98% analytical reagent (AR)), $NaNO_3$, H_2O_2 (30% AR), NaOH, acetic acid, KOH, HCl, $KMnO_4$, benzene, $NaClO_2$, and ethanol were purchased from Sinopharm Chemical Reagent Co., Ltd. (China). Banana petiole fiber powder (100 mesh) was provided by Dongyitex, Ltd. (Yunnan Province, China).

Methods

Preparation of CNF suspension

The CNF suspension was prepared by a modified method by Chen *et al.* (2011). Banana petiole fiber powder (10 g) was extracted with an ethanol and benzene (v/v = 1:2) solution at 90 °C for 6 h in a Soxhlet apparatus to remove organic soluble extractives. In order to remove water soluble extractives and pectic substances, the dried and extracted sample was treated with a mixture of 1% NaOH and H_2O_2 at 90 °C for 2.5 h, followed by 2% NaOH at 90 °C for 2.0 h. Lignin was removed from the insoluble residue by further treatment with 0.9% $NaClO_2$ and acetic acid at 75 °C for 3.0 h, which was followed by 3% KOH extraction at 90 °C for 2.0 h. Every treatment was performed with vigorous

stirring, and the insoluble residue at each step was extensively washed with distilled water until the pH of the filtrate was neutral.
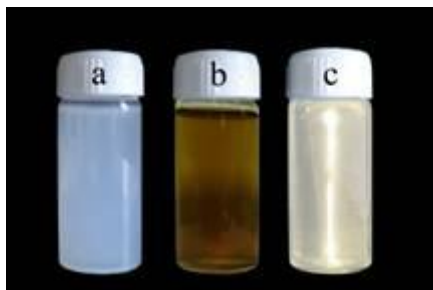
Fig. 1. Photographs of the samples: (a) ultrasonicated CNF suspension, (b) GO colloid, and (c) mixture of (a) and (b)

After the chemical pretreatments, the obtained residual slurry was diluted to 1 wt% and passed through a grinder (MKCA6-3, Masuko Corp.; Japan) at 1,500 rpm for 30 times; afterwards, the residual slurry was diluted to about 0.1 wt%. Each 250-mL diluted sample was ultrasonicated in an ice-cooled bath for 40 min by an ultrasonic generator (XO-1200, Xianqu Biological Technology Co., Ltd.; China) that operated at frequency of 20 to 25 kHz and power output of 80 W. The obtained CNF suspension is shown in Fig. 1a.

Preparation of GO colloid

Expanded graphite (EG) was prepared according to the method in the literature with minor modifications (Chen *et al.* 2012). Natural graphite powder (3 g) was dried at 80 °C for 8 h and then treated with a mixture of concentrated H_2SO_4 (150 mL) and H_2O_2 (12 mL) with vigorous stirring at 35 °C for 1.5 h to form the graphite intercalated compound (GIC). The GIC was diluted with distilled water (800 mL) with stirring for 0.5 h, which was then filtered and thoroughly rinsed with distilled water until the pH of the filtrate was neutral. After drying at 80 °C for 24 h, the GIC was treated at high temperature in a vacuum tube furnace (OTF-1200X-80-I-F3LV, Hefei Kejing Materials Technology Co., Ltd.; China) in an argon atmosphere (99.999%) at 1000 °C to synthesize the EG. The GO was synthesized from the obtained EG by a modification to the method of Hummers and Offenman (1958). The EG was vigorously stirred for 0.5 h, which was cooled in an ice bath, in a solution of concentrated H_2SO_4 (100 mL), $NaNO_3$ (1 g), and $KMnO_4$ (12 g). Afterwards, this mixture was heated to 35 °C for 4 h, and then heated to 60 °C for 3 h with stirring. The treated material was allowed to cool to room temperature for 24 h and the insoluble residue was washed with 5 wt% HCl. After centrifugal separation and dialysis, the insoluble residue was further washed with distilled water until the pH of the filtrate was neutral, which resulted in the GO. The GO colloid, as shown in Fig. 1b, was prepared by ultrasonicating the GO water dispersion (4 mg/mL) for 2 h at a power of 80 W and at a frequency of 20 to 25 kHz.

Fabrication of the films

According to the designated GO loading levels listed in Table 1, the prepared CNF suspension and the GO colloid were mixed and then ultrasonicated at 80 W power for 40 min to prepare the GO/CNF suspension, as shown in Fig. 1c. The thin wet mats

were obtained by filtrating the prepared suspension through a cellulose acetate nanoporous membrane filter, which had a diameter of 100 mm and aperture of 0.22 μm, under a vacuum; the resulting wet CNF mats were dried at 80 °C for 48 h. The CNF film and the GO/CNF film are shown in Fig. 2.
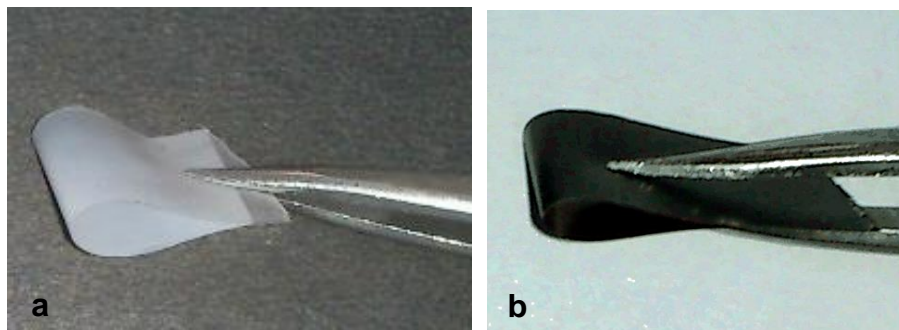
Fig. 2. Photographs of the films: (a) CNF film, and (b) GO/CNF film with 7.14 wt% GO

Characterization

The Fourier-transform infrared (FTIR) analysis was performed using a Nicolet iS10 spectrometer (Thermo Scientific Inc., USA) equipped with a single reflection attenuated total reflectance system to collect detailed information of the functional groups of the prepared CNF film (Table 1, Film No. A), GO/CNF film (Table 1, Film No. C), graphite powder, and GO. All sample spectra were collected through an accumulation of 64 scans with a resolution of 4 cm^{-1}. Raman spectra of the GO were recorded with a Thermo DXR (Thermo Fisher, USA). A laser operating at a 532 nm wavelength was applied as the light source for the excitation of Raman scattering. The spectra were recorded over a range of 500 to 3300 cm^{-1} using an operating spectral resolution of 2 cm^{-1} and a laser power output of 10 mW. The confocal aperture and slit width were 900 μm and 50 μm, respectively. The acquisition time and preview time was 6 seconds and 1 second, respectively. Atomic force microscopy (AFM) images were obtained by using a Dimension Edge microscope (Bruker, Germany). The GO solution (~0.04 mg/mL) was prepared by dropping onto a fresh mica sheet, which was dried in air. Freeze-dried cellulose nanofibers and the cross sections of the prepared films were performed on a scanning electron microscope (SEM) (S-4800, HITACHI; Japan) at an accelerating voltage of 3 kV. All samples were coated with a thin layer of gold for 30 to 60 s. Tensile strength of the films was performed with a universal testing machine (SANS, Sans Materials Testing Co., Ltd.; China) at a constant crosshead speed of 1 mm/min and a load cell of 100 N; the test sample size was 35 mm × 3 mm (length × width), with a nominal thickness of 50 μm. Before testing, all samples were conditioned at 23 ± 5 °C and 50% ± 1% relative humidity for 24 h. All measurements were done with three replicates. The thermogravimetric analysis (TGA) was performed to evaluate the degradation characteristics of the films using a thermogravimetric analyzer (Netzsch 209F1, Germany) from room temperature to 600 °C, with a heating rate of 10 °C/min under N$_2$ (20 mL/min). A sample of 10 mg was used for each run. Dynamic-mechanical analysis (DMA) was conducted with a Netzsch DMA 242Dm (Germany) tester at a frequency of 1 Hz and maximum amplitude of 30 μm in the stretch mode. The sample dimensions were 15 mm × 3.5 mm, with a nominal thickness of 50 μm. The DMA operated at a temperature range of 20 to 180 °C, and at a heating rate of 5 °C/min under a dry nitrogen atmosphere.

RESULTS AND DISCUSSION

FTIR Spectroscopy Analysis

Figure 3 shows the FTIR spectra of various samples. The GO (Fig. 3b) had characteristic infrared absorption peaks when compared to the natural graphite sample (Fig. 3a), mostly because of the oxygen groups added to the GO (Acik *et al.* 2010). The shoulder peak at 1720 cm^{-1} indicated the presence of C=O moieties in its structure, which are common in carboxylic acid, ketone, and quinone functional groups. The bands at 1619 cm^{-1} and 1376 cm^{-1} could be associated with the flexural vibration of the -OH or the skeletal vibration of the aromatic C=C groups, and the –OH deformation vibration of the –OH in –COOH groups, respectively. The bands at 1232 cm^{-1} and 1049 cm^{-1} represented the stretching vibrations of the C-OH and the C-O-C groups, respectively.
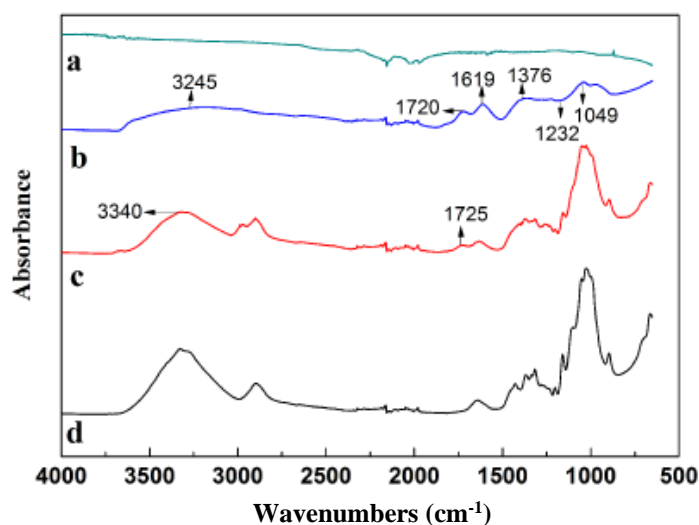
Fig. 3. FTIR spectra of samples: (a) graphite powder, (b) GO, (c) GO-treated CNF film with 4.40 wt% GO, and (d) CNF film

In addition, the broadened band of –OH stretching at 3500 to 2750 cm^{-1} was also observed in the spectra of the GO (Fig. 3b), CNF film (Fig. 3d) and GO-treated CNF film (Fig. 3c). Compared with the CNF film, both GO and GO-treated CNF film presented a C=O stretching peak at 1725 cm^{-1}. In addition, the spectra of GO-treated CNF film also showed a broadened band at 3340 cm^{-1}, indicating that the stretching vibration of C=O of GO was disturbed by the -OH of nanocellulose. This observation is in accordance with the results of Feng *et al.* (2012).

Raman Spectroscopy Analysis

Raman spectroscopy can provide valuable information regarding graphitic structure and has been proven to be an essential tool to characterize graphite and graphene materials (Tang *et al.* 2012; Li. *et al.* 2012; Yadav *et al.* 2013). In Fig. 4, the spectrum of natural graphite showed an intensive emission peak at 1565 cm^{-1} (G-band) and a very weak band at 1341 cm^{-1} (D-band). However, the G-band of GO broadened and shifted to 1587 cm^{-1}, and the D-band at 1346 cm^{-1} became much more prominent.

The G-band corresponds to an E_{2g} mode of graphite, which is related to the vibration of the sp^2 bonded carbon atoms. On the other hand, the D-band is a ring breathing mode of k-point phonons of A_{1g} symmetry, which is associated with the vibrations of carbon atoms with dangling bonds in plane terminations of disordered graphite (Li *et al.* 2012; Tang *et al.* 2012). The intensity ratio of the two bands (ID/IG) is commonly used to express the sp^2/sp^3 carbon ratio, which is a measure of the extent of disorder (Eigler *et al.* 2012). Herein, it increased from 0.05 for natural graphite to 0.92 for GO, which indicated the reduction in size of the in-plane sp^2 domains. This was due to the extensive oxidation of the graphite (Yadav *et al.* 2013).
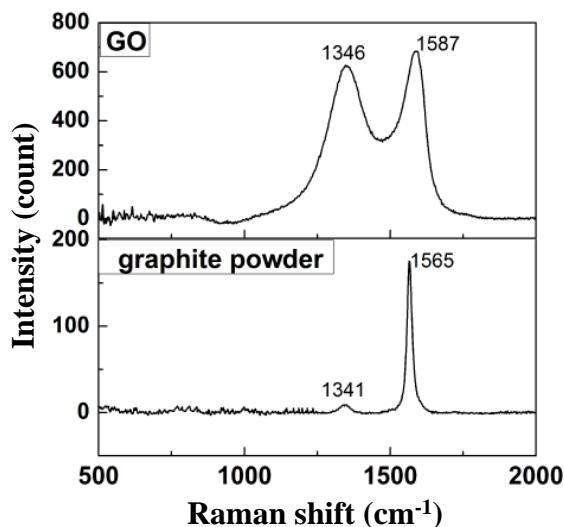

Fig. 4. Raman spectra of the graphite and the GO samples

Morphology of the Films

As shown in Fig. 5, the thickness of GO sheets measured by AFM was 0.6 to 0.9 nm, which demonstrates that the GO was exfoliated into a single layer.

Figure 6, parts a and b, shows SEM images of cellulose nanofibers that were prepared by freeze drying the nanocellulose suspension, The low magnification SEM images (Fig. 6a) revealed that the surfaces of the nano fiber were clear and they had a consistent direction of orientational alignment. During the process of freeze-drying, the water between cellulose fiber was gradually removed by sublimation. At the same time, under the effect of hydrogen bonds between them, the cellulose became arranged in an axial pattern (Chen *et al.* 2011b). Figure 6 b shows that the diameter of the fiber was around 100 nm. The SEM images (Fig. 6, parts c through h) were taken at the fractured surfaces of samples after tensile testing fracture.

For all samples, the cross-sections showed grooves of different magnitudes, which were caused by the different structure and stiffness between the cellulose and the GO. The layered structure was due to the directional flow induced by vacuum filtration during the process of film forming. In addition, there was barely a full GO sheet available in the cross-sections, indicating that the GO sheets were almost covered by the cellulose layers within the matrix, which shows a good adhesion between cellulose and GO. This result was consistent with the research of Han *et al.* (2011a,b).
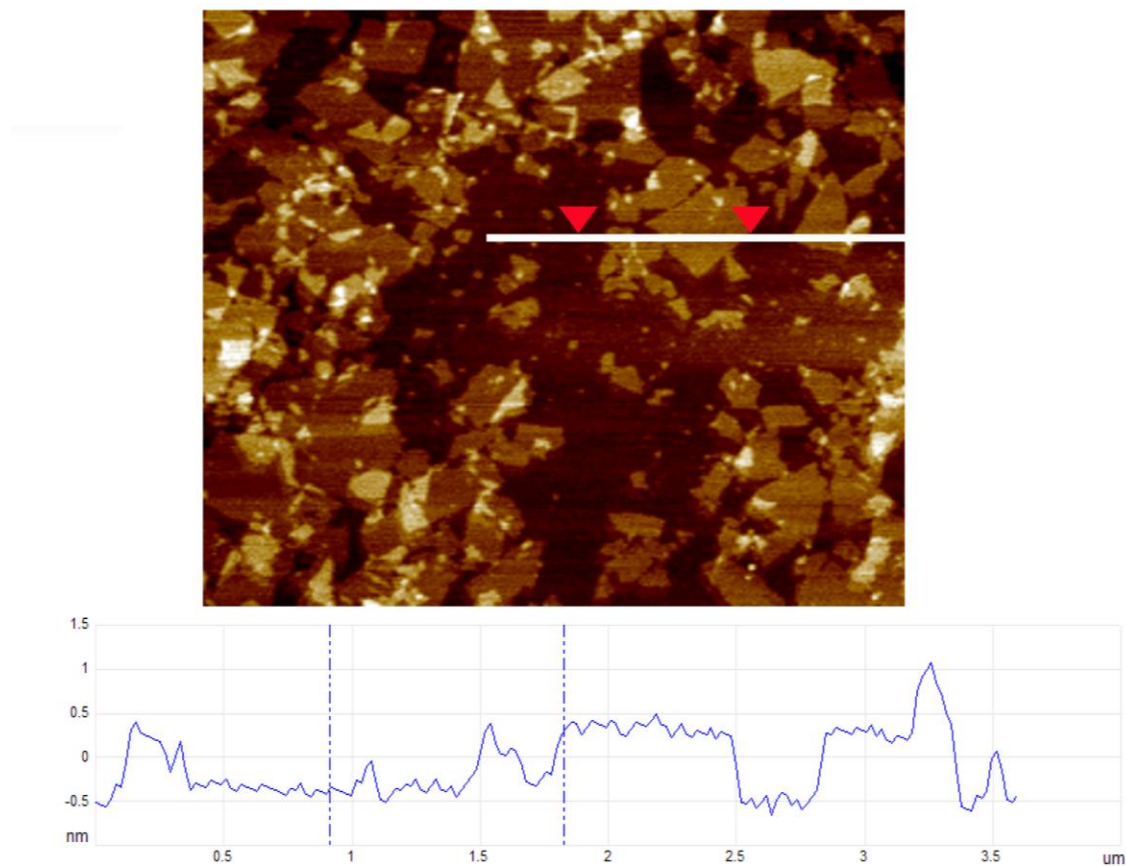
Fig. 5. AFM image and the corresponding height profile of GO

The fracture surface of the CNF film (Figs. 6c and 6d) displayed a uniform, non-porous structure from the interior to the surface, which had a dense and homogeneous texture. However, the fracture surface of the GO/CNF film with 4.4 wt% GO (Figs. 6e and 6f) was rougher but without any aggregations of GO, which revealed that the GO was well dispersed within the cellulose matrix and that the adhesion between CNFs as well as GO sheets was strong enough to be favorable for stress transfer to both components. It should be noted that both GO sheets and CNFs have individually good mechanical properties, and the good adhesion between them would show an improvement in properties of the forming composite materials (Luong *et al.* 2011).

In the GO/CNF film with 4.4 wt% GO, GO sheets and CNFs were evenly dispersed into one another and were bonded strongly to one another through hydrogen bonding and chemical bonding, which was confirmed by FTIR. This bonding led to an improvement in mechanical properties of the films. On the other hand, the film with 8.45 wt% GO (Figs. 6g and 6h) exhibited more severe aggregation of GO, which showed poor interfacial adhesion between the GO and the cellulose. Such aggregation would result in the slipping of GO sheets, which results in the failure to transfer the load from the cellulose matrix to the GO sheets. This consequently reduced the treatment capability of the GO (Wang *et al.* 2012; Yadav *et al.* 2013).
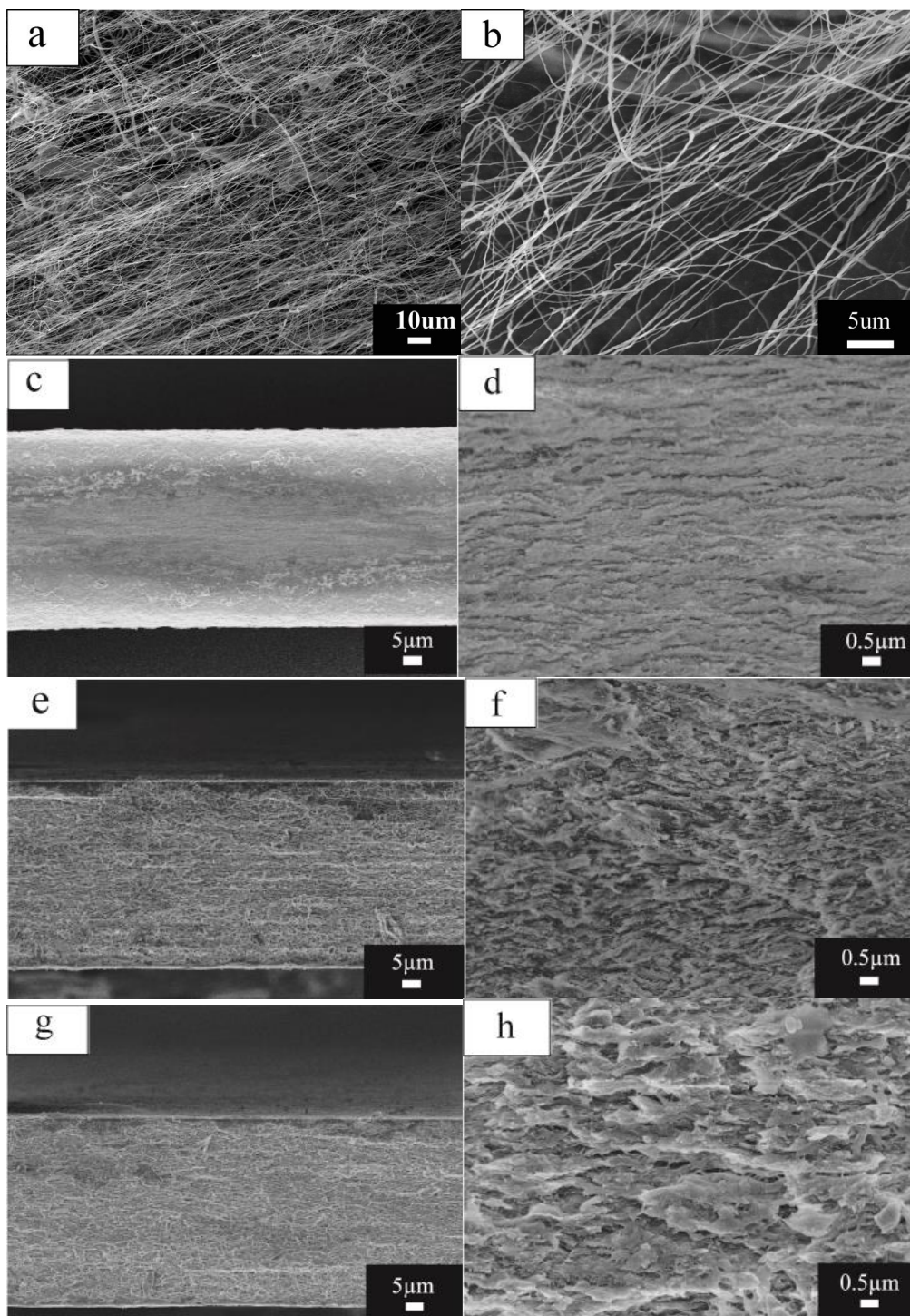
Fig. 6. SEM images of freeze-dried cellulose nanofibers (a,b) and cross-section SEM images of GO-treated CNF films with different GO loading: (c) 0.0 wt% GO loading, (d) higher magnification of 0.0 wt% GO loading, (e) 4.4 wt% GO loading, (f) higher magnification of 4.4 wt% GO loading, (g) 8.45 wt% GO loading, and (h) higher magnification of 8.45 wt% GO loading

Tensile Properties

As shown in Table 1, the tensile strength (TS) of the GO-treated films varied as influenced by the GO loading. It increased from 92.9 to 140.9 MPa when the GO content

increased from 0 to 4.4 wt%, which clearly indicated that a small amount of GO improved the TS of the films (Film Nos. A, B, and C; Table 1). However, the TS decreased when the GO loading was increased beyond 4.4 wt% (Film Nos. C, D, and E; Table 1), which showed a GO loading threshold for maximum TS. When the GO loading was lower than the threshold, the addition of GO effectively improved TS. The strong dependence of TS on the GO loading is due to the dispersion of GO into the composite matrix at the molecular level, which led to strong hydrogen bond interactions between the cellulose fibers and the surfaces of the GO (Han *et al.* 2011a). In addition, the homogeneous dispersion of GO in the cellulose matrix and the interaction of adjacent cellulose between the cellulose-GO sheets through entanglement caused a good load transfer among those phases.

When the GO loading was higher than the threshold, the TS did not increase further. The limitation of the enhancement in TS may be caused by the agglomeration of the GO sheets at the nano scale within the composite. The interactions between GO and cellulose made the composites stronger but more brittle. This result was illustrated by the SEM analysis (Fig. 5), and was consistent with the reported observations of Luong *et al.* (2011) and Han *et al.* (2011b).

The Young's moduli of the films increased with the GO loading, which revealed there was no GO loading threshold limit. This observation is consistent with reports by Han *et al.* (2011a,b), Kim *et al.* (2011), and Yadav *et al.* (2013).

**Table 1.** Mean Tensile Properties of Prepared Films

Film No.	GOLoading (wt%)	TS (MPa)	Young's Modulus (MPa)	Film Thickness (μm)
A	0	92.9 (8.8)	3859.8 (731.1)	46 (1)
B	2.98	124.7 (4.4)	4156.8 (602.5)	48 (2)
C	4.40	140.9 (4.2)	4592.5 (631.6)	50 (1)
D	7.14	85.8 (4.2)	4759.4 (414.8)	57 (2)
E	8.45	73.3 (5.5)	4819.6 (222.3)	56 (2)

*Note: Values in parentheses are standard deviation ($n = 3$)

Thermogravimetric Analysis

Figure 7 shows that the incorporation of GO into the cellulose-based composite slightly enhanced the thermal stability of the composite. The TG-DTG diagram of the CNF film presented a conspicuous weight loss in the temperature range of 25 to 100 °C, which was attributable to the water lost within the matrix (Yousefi *et al.* 2013); however, the values for the GO/CNF film (B, C, D, E) only had a slight decline at about 50 °C, which suggested that the water content within this composite film was lower than that of the CNF film. However, the GO/CNF film lost its weight sharply at 340 °C, which was a little higher than that of the CNF film (336 °C). After the sharp pyrolysis of the cellulose, the GO/CNF film revealed a moderate decomposition, which was attributed to the strong interaction between GO and cellulose (Yao *et al.* 2014). The decomposition temperature of 387 °C for the GO/CNF film was also higher than that of the CNF film, which demonstrated the better thermal stability of this film at a high temperature. The char

residues after decomposition (600 °C) of the CNF film and the GO/CNF films were 20%, 24%, 26%, 29%, respectively.
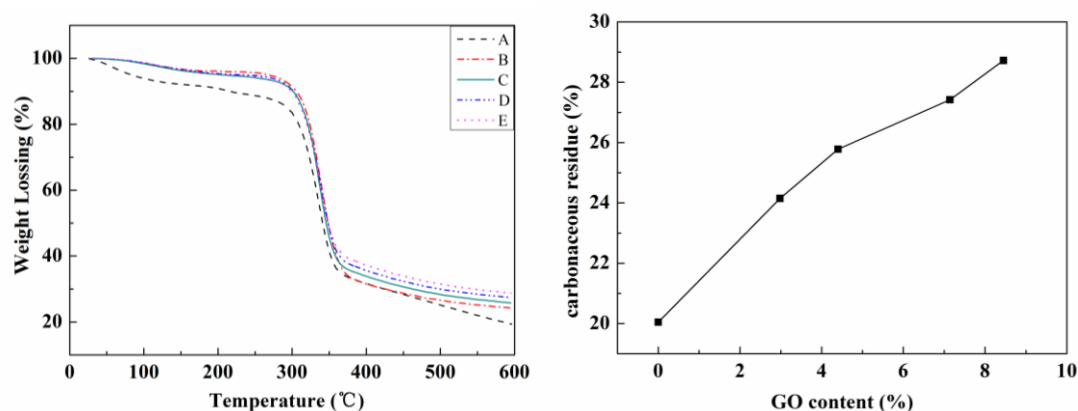
Fig. 7. TG curves of the (A) CNF film and (B,C,D,E) GO/CNF film, and the carbonaceous residue at 600 °C of all films
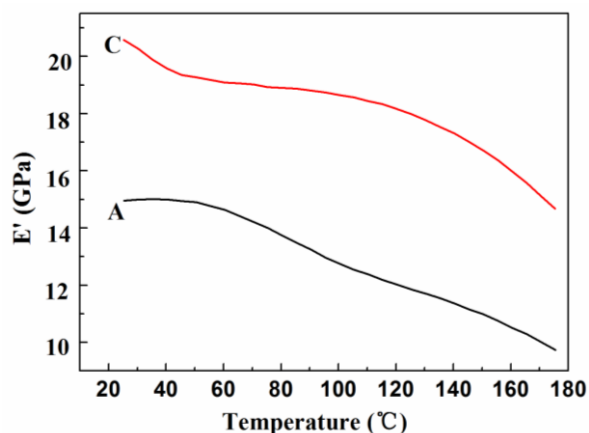
Fig. 8. Storage modulus of the (A) CNF film and (C) GO/CNF film

Variations of storage modulus (E') of non-treated (Film No. A; Table 1) and GO-treated CNF films (Film No. C; Table 1) are shown in Fig. 8. The E' value of the films decreased with the increasing temperature, regardless of the GO loading. As the temperature increased from 25 °C to 175 °C, the E' value of the CNF film decreased from 14.95 GPa to 9.66 GPa; however, the E' value for the CNF film decreased from 20.57 GPa to 14.67 GPa. This suggested that the interactions between the CNF and the GO in the composite matrix were strong. The retention ratio, defined as E'(175 °C)/E'(25 °C), was 0.65 and 0.71 for the CNF film (A) and the GO/CNF film (C), respectively. Apparently, the GO-treated film had a higher E' and a retention ratio than the non-treated one, which confirmed that the GO treatment improved the mechanical properties at high temperatures. Such behavior has been reported for chitosan/GO nanocomposite films (Han *et al.* 2011a) and sodium carboxymethyl cellulose/GO nanocomposite film (Yadav *et al.* 2013).

CONCLUSIONS

1. The GO-treated CNF film was synthesized from banana petiole and natural graphite in a simple ultrasonic mixing method to combine the GO colloid and the CNF suspension. The GO loading level in the CNF composite films dramatically affected properties of the films. The tensile moduli increased with GO loading up to 4.4 wt%; higher GO loading levels caused the tensile strength of the composite to decrease.

2. The FTIR and SEM image analyses illustrated that the GO was dispersed to a great degree within the CNF matrix and that the GO interacted with CNF through intermolecular hydrogen bonds, which afforded good mechanical properties of the film at the lower GO loading levels. However, higher GO loading levels had a negative effect on tensile strength, which was caused by GO agglomeration and heterogeneity within the CNF matrix, or by discontinuity of the composite film structure.

3. The TGA and DMA results suggested that the GO-treated films had higher storage moduli, retention ratios, and amounts of char remaining after pyrolysis. GO was shown to be a good filler for cellulose film. GO/CNF film may be a suitable material for heat-resistant material or high strength flexible folding material.

ACKNOWLEDGMENTS

REFERENCES CITED

Acik, M., Mattevi, C., Gong, C., Lee, G., Cho, K., Chhowalla, M., and Chabal, Y. J. (2010). "The role of intercalated water in multilayered graphene oxide," *ACS Nano*. 4(10), 5861-5868. DOI: 10.1021/nn101844t

Chen, W., Yu, H., Liu, Y., Chen, P., Zhang, M., and Hai, Y. (2011a). "Individualization of cellulose nanofibers from wood using high-intensity ultrasonication combined with chemical pretreatments," *Carbohyd. Polym.* 83(4), 1804-1811. DOI: 10.1016/j.carbpol.2010.10.040

Chen, W., Yu, H., and Liu, Y. (2011b). "Preparation of millimeter-long cellulose I nanofibers with diameters of 30–80 nm from bamboo fibers," *Carbohyd. Polym.* 86(2), 453-461. DOI: 10.1016/j.carbpol.2011.04.061

Chen, C., Huang, J., Zhang, Q., Gong, W., Yang, Q., Wang, M., and Yang, Y. (2012). "Annealing a graphene oxide film to produce a freestanding high conductive graphene film," *Carbon* 50(2), 659-667. DOI: 10.1016/j.carbon.2011.09.022

Deepa, B., Abraham, E., Cherian, B. M., Bismarck, A., Blaker, J. J., Pothan, L. A., Leao, A. L., Souza, S. F., and Kottaisamy, M. (2011). "Structure, morphology and thermal characteristics of banana nano fibers obtained by steam explosion," *Bioresour. Technol.* 102(2), 1988-1997. DOI: 10.1016/j.biortech.2010.09.030

Elanthikkal, S., Gopalakrishnapanicker, U., Varghese, S., and Guthrie, J. T. (2010). "Cellulose microfibres produced from banana plant wastes: Isolation and characterization," *Carbohyd. Polym*. 80(3), 852-859. DOI: 10.1016/j.carbpol.2009.12.043

Eigler, S., Dotzer, C., and Hirsch, A. (2012). "Visualization of defect densities in reduced graphene oxide," *Carbon* 50(10), 3666-3673. DOI: 10.1016/j.carbon.2012.03.039

Feng, Y., Zhang, X., Shen, Y., Yoshino, K., and Feng, W. (2012). "A mechanically strong, flexible and conductive film based on bacterial cellulose/graphene nanocomposite," *Carbohyd. Polym.* 87(1), 644-649. DOI: 10.1016/j.carbpol.2011.08.039

Gao, K. Z., Shao, Z. Q., Wu, X., Wang, X., Li, J., *et al*. (2013). "Cellulose nanofibers /reduced graphene oxide flexible transparent conductive paper," *Carbohyd. Polym.* 97, 243-251. DOI: 10.1016/j.carbpol.2013.03.067

Han, D. L., Yan, L., Chen, W., and Li, W. (2011a). "Preparation of chitosan/graphene oxide composite film with enhanced mechanical strength in the wet state," *Carbohydr. Polym.* 83(2), 653-658. DOI: 10.1016/j.carbpol.2010.08.038

Han, D. L., Yan, L. F., Chen, W. F., Li, W., and Bangal, P. R. (2011b). "Cellulose/ graphite oxide composite films with improved mechanical properties over a wide range of temperature," *Carbohyd. Polym.* 83(2), 966-972. DOI: 10.1016/j.carbpol.2010.09.006

Hummers, W. S., and Offenman, R. E. (1958). "Preparation of graphitic oxide," *J. Am. Chem. Soc*. 80(6), 1339. DOI: 10.1021/ja01539a017

Jandas, P. J., Mohanty, S., and Nayak, S. K. (2013). "Surface treated banana fiber reinforced poly (lactic acid) nanocomposites for disposable applications," *J. Clean Prod.* 52(1), 392-401. DOI: 10.1016/j.jclepro.2013.03.033

Kim, C. J., Khan, W., Kim, D., Cho, K., and Park, S. (2011). "Graphene oxide/cellulose composite using NMMO monohydrate," *Carbohydr. Polym.* 86(2), 903-909. DOI: 10.1016/j.carbpol.2011.05.041

Kovtyukhova, N. I., Ollivier, P. J., Martin, B. R., Mallouk, T. E., Chizhik, S. A., Buzaneva, E. V., and Gorchinskiy, A. D. (1999). "Layer-by-layer assembly of ultrathin composite films from micro-sized graphite oxide sheets and polycations," *Chem. Mater*. 11(3), 771-778. DOI: 10.1021/cm981085u

Lim, H. N., Huang, N. M., and Loo, C. H. (2012). "Facile preparation of graphene-based chitosan films: Enhanced thermal, mechanical and antibacterial properties," *J. Non-Cryst. Solids.* 358, 525-530. DOI: 10.1016/j.jnoncrysol.2011.11.007

Li, J. H., Kuang, D. Z., Feng, Y. L., Zhang, F. X., Xu, Z. F., and Liu, M. Q. (2012). "A graphene oxide-based electrochemical sensor for sensitive determination of 4-nitrophenol," *J. Hazard Mater*. 201-202, 250-259. DOI: 10.1016/j.jhazmat.2011.11.076

Luong, N. D., Pahimanolis, N., Hippi, U., Korhonen, J. T., Ruokolainen, J., Johansson, L. S., Nam, J. D., and Seppälä, J. (2011). "Graphene/cellulose nanocomposite paper with high electrical and mechanical performances," *J. Mater. Chem*. 21, 13991-13998. DOI: 10.1039/C1JM12134K

Paredes, J. I., Villar-Rodil, S., Martinez-Alonso, A., and Tascón, J. M. D. (2008). "Graphene oxide dispersions in organic solvents," *Langmuir* 24(19), 10560-10564. DOI: 10.1021/la801744a

Park, S., Lee, K., Bozoklu, G., Cai, W., Nguyen, S. T., and Ruoff, R. S. (2008). "Graphene oxide papers modified by divalent ions-Enhancing mechanical properties via chemical cross-linking," *ACS Nano* 2(3), 572-578. DOI: 10.1021/nn700349a.

Shao, G., Lu, Y., Wu, F., Yang, C., Zeng, F., and Wu, Q. (2012). "Graphene oxide: The mechanisms of oxidation and exfoliation," *J. Mater Sci*. 47(10), 4400-4409. DOI: 10.1007/s10853-012-6294-5

Tang, L., Li, X., Du, D., and He, C. J. (2012). "Fabrication of multilayer films from regenerated cellulose and graphene oxide through layer-by-layer assembly," *Prog. Nat. Sci.* 22(4), 341-346. DOI: 10.1016/j.pnsc.2012.06.005

Wang, Y., Xie, L., Sha, J., Ma, Y., Han, J., Dong, S., Liu, H., Fang, C., Gong, S., and Wu, Z. (2011). "Preparation and chemical reduction of laurylamine-intercalated graphite oxide," *J. Mater Sci*. 46(10), 3611-3621. DOI:10.1007/s10853-011-5277-2.

Wang, B. G., Lou, W. J., Wang, X. B., and Hao, J. C. (2012). "Relationship between dispersion state and reinforcement effect of graphene oxide in nanocrystalline cellulose-graphene oxide composite films," *J. Mater. Chem*. 22(25), 12859-12866. DOI: 10.1039/C2JM31635H

Wang, J. J., Miao, F., and Zhan, H. B. (2014). "Preparation, characterization, and nonlinear optical properties of graphene oxide-carboxymethyl cellulose composite films," *Optics & Laser Technology* 57, 84-89. DOI: 10.1016/j.optlastec.2013.09.040

Yadav, M., Rhee, K. Y., Jung, I. H., and Park, S. J. (2013). "Eco-friendly synthesis, characterization and properties of a sodium carboxymethyl cellulose/graphene oxide nanocomposite film," *Cellulose* 20(2), 687-698. DOI: 10.1007/s10570-012-9855-5

Yao, L., Lu, Y., Wang, Y., and Hu, L. (2014). "Effect of graphene oxide on the solution rheology and the film structure and properties of cellulose carbamate," *Carbon* 69(April 2014), 552-562. DOI: 10.1016/j.carbon.2013.12.066

Yousefi, H., Faezipour, M., Hedjazi, S., Mousavi, M. M., Azusa, Y., and Heidari, A. H. (2013). "Comparative study of paper and nanopaper properties prepared from bacterial cellulose nanofibers and fibers/ground cellulose nanofibers of canola straw," *Ind. Crops Prod*. 43, 732-737. DOI: 10.1016/j.indcrop.2012.08.030

Zuluaga, R., Putaux, J. L., Cruz, J., Vélez, J., Mondragon, I., and Gañán, P. (2009). "Cellulose microfibrils from banana rachis: Effect of alkaline treatments on structural and morphological features," *Carbohyd. Polym.* 76(1), 51-59. DOI: 10.1016/j.carbpol.2008.09.024